LBL-23023
Preprint c.2

Lawrence Berkeley Laboratory

UNIVERSITY OF CALIFORNIA

EARTH SCIENCES DIVISION

RECEIVED
LAWRENCE
BERKELEY LABORATORY

APR 22 1987

LIBRARY AND
DOCUMENTS SECTION

Submitted to International Journal of Heat
and Mass Transfer

A SEMIANALYTICAL SOLUTION FOR HEAT PIPE EFFECTS NEAR HIGH-LEVEL NUCLEAR WASTE PACKAGES BURIED IN PARTIALLY SATURATED GEOLOGICAL MEDIAS

C. Doughty and K. Pruess

February 1987

TWO-WEEK LOAN COPY

This is a Library Circulating Copy which may be borrowed for two weeks.

LBL-23023 c.2

Prepared for the U.S. Department of Energy under Contract DE-AC03-76SF00098

DISCLAIMER

This document was prepared as an account of work sponsored by the United States Government. While this document is believed to contain correct information, neither the United States Government nor any agency thereof, nor the Regents of the University of California, nor any of their employees, makes any warranty, express or implied, or assumes any legal responsibility for the accuracy, completeness, or usefulness of any information, apparatus, product, or process disclosed, or represents that its use would not infringe privately owned rights. Reference herein to any specific commercial product, process, or service by its trade name, trademark, manufacturer, or otherwise, does not necessarily constitute or imply its endorsement, recommendation, or favoring by the United States Government or any agency thereof, or the Regents of the University of California. The views and opinions of authors expressed herein do not necessarily state or reflect those of the United States Government or any agency thereof or the Regents of the University of California.

LBL-23023

A Semianalytical Solution for Heat Pipe Effects Near High-Level Nuclear Waste Packages Buried in Partially Saturated Geological Media

Christine Doughty and Karsten Pruess

Earth Sciences Division
Lawrence Berkeley Laboratory
University of California
Berkeley, California 94720

February 1987

This work was supported by the
U.S. Department of Energy under Contract No.DE-AC03-76SF0098

A Semianalytical Solution for Heat Pipe Effects near High-Level Nuclear Waste Packages Buried in Partially Saturated Geological Media

Christine Doughty and Karsten Pruess
Earth Sciences Division
Lawrence Berkeley Laboratory

Abstract

The emplacement of a strong heat source, such as a high-level nuclear waste package, in a partially saturated permeable medium will give rise to the development of heat pipe conditions. The present paper analyzes a suitably simplified version of this problem which has a steady-state solution, for radial geometry. The solution is obtained in semianalytical form, and is compared to the analogous solution for a linear heat pipe. Various applications are presented for porous as well as for fractured-porous media with different hydrologic properties. The parameters determining heat pipe length and the question of whether or not the vicinity of the heat source dries up are discussed. The semianalytical solution is verified by means of numerical simulations which show the transient evolution from uniform initial conditions to the eventual steady state.

Nomenclature

f	dimensionless capillary pressure ($f = P_{cap} / P_{c0}$)
f'	derivative of f with respect to S
g	gravitational acceleration (m/s^2)
h_{vl}	vaporization enthalpy (J/kg)
K	thermal conductivity (W/m K)
k	intrinsic permeability (m^2)
k_r	relative permeability
$\dot{m}$	mass flow rate per unit area (kg/s m^2)
P	gas pressure (Pa)
P_a	partial pressure of air (Pa)
P_v	partial pressure of vapor (Pa)
P_l	liquid pressure (Pa)
P_{cap}	capillary pressure (Pa) ($P_{cap} = P_l - P_g$)
P_{c0}	reference capillary pressure (Pa)
P_{sat}	saturation pressure (Pa)
Q	heat source strength (W/m)
q	heat flux (W/m^2) ($q = Q / 2\pi r$ in radial geometry)
R	gas constant for water (461.52 J/kg K)
r	radial distance (m)
dr	radial mesh spacing (m)
Δr	heat-pipe length (m)
S_l	liquid saturation
S_{lr}	irreducible liquid saturation
S_{ls}	saturation at which liquid becomes fully mobile
S	scaled liquid saturation ($S = (S_l - S_{lr})/(S_{ls} - S_{lr})$)
T	temperature (°C)
x_0	heat-pipe length in linear geometry (m)
Y	Air mole fraction

Greek Symbols

β	ratio of kinematic viscosity for liquid and vapor
δ	dimensionless distance (eq. A.11)
λ	parameter in characteristic curves
ν	kinematic viscosity (m^2/s)
ρ	density (kg/m^3)
σ	vapor-liquid interfacial tension (N/m)
ϕ	porosity
ψ	function controlling heat pipe length
ω	dimensionless heat source strength (eq. A.12)

Subscripts

a	air
b	outer boundary of system
c	waste canister
f	fracture
g	gas
i	inner boundary of heat pipe
l	liquid
o	outer boundary of heat pipe
v	vapor

Introduction

Heat pipes are being widely applied in engineered heat transfer systems, and various aspects of their behavior have been studied by many workers. The basic ingredients of a heat pipe are (1) a volatile fluid, and (2) a mechanism by which liquid and gas phases can flow in opposite directions. If heat is injected into such a system, liquid phase will vaporize, causing pressurization of the gas phase and gas-phase flow away from the heat source. The vapor condenses in cooler regions away from the heat source, depositing its latent heat of vaporization there. This sets up a saturation profile, with liquid phase saturations increasing away from the heat source. In engineered heat pipe systems incorporating porous media, backflow of the liquid phase towards the heat source is effected by capillary forces. Heat pipes occur naturally on a large scale (kilometers) in a rare type of hydrothermal convection system known as vapor-dominated geothermal reservoirs [1, 2, 3]. In these systems a deep heat source of magmatic origin vaporizes water present in fractured porous rocks. The vapor rises in the fractures, and condenses at shallower depths on the cooler rock surfaces. The liquid condensate then flows back towards the heat source simply by gravitational force. Effective heat conductivity in these systems can be of the order of several hundred W/m °C, whereas heat conductivity of rocks is typically in the range of 1-3 W/m °C.

A number of workers have developed analytical and semianalytical solutions for the steady state behavior of one-dimensional heat pipes in homogeneous porous media [4, 5, 6, 7, 8]. All the formulations assume a linear one-dimensional geometry, and some include gravity.

In the present paper we study a problem which arises in the context of nuclear waste isolation, namely, a heat pipe in one-dimensional radial (cylindrical) geometry. Numerical simulation studies by Pruess, Tsang, and Wang [9] have indicated that strong heat pipe effects can evolve in the vicinity of high-level nuclear waste packages buried in a partially saturated permeable material. This is of great practical significance, as it

may have dramatic impacts on waste package environment and design criteria (temperatures, presence or absence of moisture and air). The conditions which may be attained at some time following high-level waste emplacement are schematically depicted in Fig. 1. The waste package may be surrounded by a dried zone, in which heat transfer occurs essentially only by conduction. At larger distance a heat pipe region may be present, beyond which there is another zone with predominantly conductive heat transfer, where temperatures are too low for significant evaporation and heat pipe effects to occur. Depending upon the properties of the permeable medium and the rate of heat input, the heat pipe region could extend all the way to the heat source, or it could be extremely short.

For the problem of geologic disposal of high-level nuclear waste, heat pipe conditions will be of a transient nature, as heat is being transferred from a localized source with a time-varying rate into a large (essentially infinite) rock mass. The problem addressed in the present paper has been simplified by assuming that (1) the rate of heat generation is constant, independent of time; and (2) time-independent boundary conditions are posed at a finite distance from the heat source. With these two simplifications the system will attain steady-state conditions, for which an approximate semianalytical solution can be obtained. Additional approximations will be introduced in the course of the theoretical formulation, below. We also report fully-transient numerical simulations of the heat pipe process near a cylindrical heat source, which are used to verify the accuracy of the semianalytical solution.

Theoretical Formulation

Present design considerations assume nuclear wastes to be packaged in tall cylinders of approximately 4.5 m length and 0.5 m diameter [10]. For vertical emplacement, this shape will give rise to two-dimensional cylindrically symmetric heat flow patterns. In order to simplify the analysis, we eliminate end effects by considering a heat

source in the form of an infinitely long string of cylindrical waste packages. Further, by neglecting gravity effects and assuming that boundary conditions depend only on radial distance r from the symmetry axis, fluid and heat flow will possess one-dimensional radial symmetry. For time-independent boundary conditions, the system will attain a steady state. Under steady state conditions, three domains with different heat transfer mechanisms may exist in the porous medium around the heat source (see Fig. 1). The innermost domain is a vapor zone in which little mass flow occurs and heat flow is conduction dominated. The middle domain is a two-phase liquid/vapor zone at the saturation temperature, the heat pipe region, where heat flow is primarily convective. The outermost domain is a liquid water/air domain at temperatures below the saturation temperature in which there is little mass flow and conduction-dominated heat flow. The variables used to describe the state of the system are gas phase pressure P, temperature T, air partial pressure P_a, and liquid saturation S_l. It is also convenient to define a scaled liquid saturation S, given by $S = (S_l - S_{lr})/(S_{ls} - S_{lr})$, where S_{lr} is the irreducible liquid saturation, and S_{ls} is the saturation at which liquid relative permeability becomes equal to 1.

A constant heat source of strength Q is prescribed at the waste canister radius r_c. The pressure, temperature, and saturation conditions are assumed fixed at a radial distance of r_b. These boundary conditions are denoted P_b, T_b, and S_{lb}, respectively. The specification of P_b and T_b fixes P_{ab}, air partial pressure at r_b, through the saturation curve. The scaled liquid saturation at the boundary is given by $S_b = (S_{lb} - S_{lr})/(S_{ls} - S_{lr})$.

In the outer conduction zone (see Fig. 1), total pressure and saturation are assumed to be equal to the boundary values. Heat flow is purely conductive, so that the temperature at a distance r can be expressed as

$$T(r) = T_b + \frac{Q}{2\pi K_b} \ln\left(\frac{r_b}{r}\right) \tag{1}$$

where K_b is the thermal conductivity of the medium at a saturation S_{lb}. The

saturation dependence of thermal conductivity for geologic media has been studied by Somerton et al. [11, 12]. The gas phase in the outer conduction zone is a mixture of air and vapor. Air partial pressure is

$$P_a = P_b - P_v \tag{2}$$

with vapor pressure P_v given by the Kelvin equation

$$P_v(T,S) = P_{sat}(T)\cdot\exp\left(\frac{P_{cap}(S)}{\rho_l R(T+273.15)}\right) \tag{3}$$

where P_{sat} is saturation pressure, P_{cap} is capillary pressure (negative), ρ_l is liquid density, and R is the gas constant for water. For weak or moderate capillary pressures, vapor pressure lowering effects are small, and the exponential factor can be replaced by 1. (A 1% lowering of vapor pressure requires a capillary pressure of approximately P_{cap}=-13 bars.)

Equation (1) shows that T steadily increases as r decreases; equation (3) indicates a corresponding increase in P_v, while a concurrent decrease in P_a follows from (2). When P_v becomes equal to total pressure P_b (and P_a=0), heat pipe conditions develop. The temperature T_o at which this occurs can be obtained from (3)

$$P_{sat}(T_o)\cdot\exp\left(\frac{P_{cap}(S_b)}{\rho_l R(T_o+273.15)}\right) = P_b \tag{4}$$

The outer boundary of the heat pipe, r_o, can be obtained by solving equation (1) for $T(r_o)=T_o$. At r_o, we have $P_o = P_b$, P_{ao}=0, and $S_o = S_b$. The variation of saturation with radial distance between r_o and the inner boundary of the heat pipe, r_i, is derived in Appendix A. The parameter r_i is determined from the condition $S_i \equiv S(r_i) = 0$.

If $r_i < r_c$ then two-phase conditions extend all the way to the heat source, and the inner conduction zone is absent. If $r_i > r_c$ then a single-phase vapor zone, in which heat transfer is conduction dominated, develops around the heat source. The value of T_c can

then be calculated from

$$T_c = T_i + \frac{Q}{2\pi K_v} \ln\left(\frac{r_i}{r_c}\right) \tag{5}$$

where T_i is the temperature at the inner boundary of the heat pipe, and K_v is the thermal conductivity of the vapor-saturated porous medium. Because K_v is small, and Q can be large, T_c can be much higher than T_i. As well as causing a large increase in T_c, the formation of a vapor zone around the heat source inhibits a number of chemical reactions that depend on the presence of liquid water.

Fluid and heat flow in the heat pipe region are considered in Appendix A. By integrating equation (A.15), the saturation profile along the heat pipe can be obtained as an implicit function of radius

$$\omega \int_{r_0}^{r} d\delta = \omega\delta(r) = \int_{S_b}^{S(r)} \frac{-f'}{\frac{1}{k_{rg}} + \frac{\beta}{k_{rl}}} dS \tag{6}$$

Equation (6) is of the same form as Udell's equation (24) [8] for linear geometry. For moderate heat flux, temperature variations along the heat pipe are small, and the integrand in (6) is primarily a function of S. It can be integrated numerically for given capillary pressure and relative permeability functions. In the examples below, we have integrated equation (6) using the **C**autious **AD**aptive **R**omberg **E**xtrapolation (CADRE) numerical integration algorithm [13]. The inner boundary of the heat pipe region, r_i, can be found by integrating (6) to $S(r_i)$=0.

$$\omega\delta(r_i) = \int_{S_b}^{0} \frac{-f'}{\frac{1}{k_{rg}} + \frac{\beta}{k_{rl}}} dS \equiv -\psi(\beta, S_b) \tag{7}$$

The function $\psi(\beta, S_b)$, which governs total heat pipe length is shown in Fig. 2 for the P_{cap}, k_{rg}, and k_{rl} functions given in Table 3, Case A and several values of S_{lb}. Substituting the definitions for ω and δ into (7) yields r_i:

$$r_i = r_o \exp\left[\frac{2\pi\psi(\beta,S_b)h_{vl}P_{c0}k}{Q\,\nu_v}\right] \tag{8}$$

where h_{vl} is the latent heat of evaporation of water, P_{c0} is a (negative) reference capillary pressure, k is intrinsic permeability, and ν_v is vapor kinematic viscosity.

The pressure profile in the heat pipe region can be similarly obtained by noting that

$$\frac{dP}{dS} = \frac{\frac{dP}{dr}}{\frac{dS}{d\delta}\cdot\frac{d\delta}{dr}} \tag{9}$$

and using (A.15) for $dS/d\delta$, (A.2) for dP/dr, and differentiating (A.11) to obtain $d\delta/dr$. Finally, equation (3) can be used to obtain temperatures from pressures.

It is of interest to state the conditions under which the vicinity of the heat source will dry up (i.e., $r_i > r_c$). From equations (1) and (8) this condition can be written, neglecting vapor pressure lowering, as

$$\exp\left\{\frac{2\pi}{Q}\left[K_b\left(T_{sat}(P_b) - T_b'\right) - \frac{\psi h_{vl}P_{c0}k}{\nu_v}\right]\right\} < \frac{r_b}{r_c} \tag{10}$$

Dry-up of the heat source is facilitated by large heat flux Q and small permeability k.

Comparison to Linear Geometry Case

For the linear geometry case with $S_b = 1$, Udell [8] obtains an expression for the length of the heat pipe x_0 given by

$$x_0 = \frac{-\psi(\beta,1)h_{vl}P_{c0}k}{q\,\nu_v} \tag{11}$$

Taking the heat flux q in the radial flow case at the inner end of the heat pipe, $q = Q/2\pi r_i$, equation (8) for r_i can be written as

$$r_i = r_o\, e^{-x_0/r_i} \tag{12}$$

The heat pipe length is

$$\Delta r = r_o - r_i = r_i (e^{x_0/r_i} - 1) \tag{13}$$

Expanding the exponential, this becomes

$$\Delta r = x_0 \left(1 + \frac{x_0}{2r_i} + \frac{x_0^2}{6r_i^2} + \cdots \right) \tag{14}$$

indicating that heat pipe length in radial geometry can be substantially larger than in linear geometry. For heat pipes far removed from the canister (r_i large) or short heat pipes (x_0 small), $(x_0/r_i) \rightarrow 0$, linear geometry is being approached, and therefore $\Delta r \rightarrow x_0$.

Examples

We have applied the above formulation to calculate steady-state thermo-hydrologic conditions near a cylindrical heat source emplaced in a partially saturated porous medium for a variety of problem parameters (see Tables 1–3). The heat source radius and strength are $r_c = 0.2$ m and $Q = 500$ W/m, respectively. At the outer boundary $r_b = 10$ m, ambient conditions of $T_b = 26\,^\circ$C, $P_b = 1$ bar, and $S_{lb} = 0.8$ prevail. In cases A–C permeability and porosity are 10^{-12} m^2 and 0.4, respectively, which is representative of a laboratory sand pack. In cases D–F we take $k = 32.6 \times 10^{-18}$ m^2 and $\phi = 0.108$, as has been suggested for Yucca mountain tuffs [10]. From equation (7) we see that the length of the heat pipe depends strongly on the relative permeability functions, k_{rg} and k_{rl}, so the different cases examine the effect of various functional forms for relative permeability. The relative permeability curves for cases A–C are shown in Fig. 3, while those for cases D–F are shown in Fig. 4. The resulting saturation, pressure, temperature, and composition profiles are given in Figs. 5–11; for convenience we have plotted air mole fraction $Y = P_a / P$ rather than partial pressure P_a.

The characteristic curves for case A have been used in conjunction with laboratory studies using packed sand cores [8, 14, 15, 16]. Case B uses the same capillary pressure function, but a linear rather than cubic saturation-dependence for relative permeabilities, as has been suggested by other workers [5, 7]. The effect of using either cubic or linear relative permeability curves is clearly seen by comparing Figs. 5 and 6. In Fig. 5 (case A, cubic relative permeabilities) the heat pipe is short enough so that a vapor zone forms around the canister, leading to high temperatures at the canister. In Fig. 6 (case B, linear relative permeabilities) the saturation decline towards the canister is more gradual, yielding a longer heat pipe region. At the canister radius, there is still liquid present, so temperature remains near the saturation temperature. The effect of relative permeability functions can be predicted qualitatively by examining equation (7) and the relative permeability curves for cases A and B (Fig. 3). The cubic relative permeabilities are smaller than the linear ones over the entire range of liquid saturation where both phases are mobile. Thus the denominator of the integrand in (7) is consistently bigger for the cubic functions, leading to a smaller value of ψ, and consequently a shorter heat pipe.

The relative permeability curves of cases A and B are commonly used in the petroleum literature, but their applicability to two-phase water flow is less well established. Case C uses relative permeabilities as measured in laboratory experiments on liquid-vapor water flow [17]. The saturation profile for case C (Fig. 7) is similar to that for case B (Fig. 6); liquid saturation remains large and no vapor zone forms at the canister. A careful examination of equation (7) and Fig. 3 indicates why this is so. The magnitude of the integrand in equation (7) is dominated by the smaller of the relative permeabilities. Fig. 3 shows that for large liquid saturations, vapor relative permeability is smaller and therefore the controlling factor in (7). Further, k_{rg} values for cases B and C are similar for large S_l, and much larger than k_{rg} for case A. Thus the saturation profiles for cases B and C are similar to each other (Figs. 6 and 7), but quite different from that for case A (Fig. 5).

For small liquid saturations, k_{rl} is smaller than k_{rg}, so k_{rl} becomes the controlling factor in equation (7). Since the k_{rl} curves are quite different for cases B and C, one would expect the resulting saturation profiles to differ for small values of S. Fig. 8 shows the heat pipe conditions for cases B and C with a larger heat flux, Q =1750 W/m. As predicted, the saturation profiles begin to deviate significantly only when S becomes small.

Case D uses characteristic curves [18] that have been suggested as plausible for the rock matrix of the candidate nuclear waste repository site at Yucca Mountain, Nevada [9, 10]. The saturation and temperature profiles (Fig. 9) show that the heat pipe is extremely short and there is no isothermal two-phase zone separating the inner and outer conduction zones. This result is supported by equation (8), which indicates that heat pipe length depends exponentially on absolute permeability k, which is much smaller for case D (32.6×10^{-18} m^2) than for cases A–C (10^{-12} m^2). It should be pointed out that the potential repository horizon at Yucca Mountain is highly fractured [10], and the case D parameters neglecting fracture effects are considered unrealistic.

Pruess et al. [9] developed an effective continuum approximation, in which fracture effects are represented by means of suitably modified relative permeability functions. Essentially, effects of large fracture permeabilities are approximated by allowing relative permeability to become very large. Following Pruess et al. [9] we have considered two effective continuum cases, E and F, which differ with respect to assumed liquid phase mobility in the fractures. Case E makes the conventional assumption that at ambient conditions of S_{lb} =80%, corresponding to a capillary pressure of P_{cap} =–10.92 bars, the fractures are drained of liquid so that the large fracture permeability is available only for gas phase flow. Fracture flow effects can then be simply represented by assigning a large constant relative permeability $k_{rg} = k_f / k$ to the gas phase, where k_f is average fracture permeability in the continuum sense. For an assumed $k_f = 10^{-13}$ m^2, we have k_{rg} =3067 (see Table 3 and [9]). Alternatively it appears possible that a finite liquid phase mobility

may be present in fractures whose bulk volume has been drained, because of liquid held on the fracture surfaces by means of phase adsorption forces, or by means of capillary effects from surface roughness. Case F uses the relative permeability parameters proposed by Pruess et al. [9] to represent mobility of both gas and liquid phases in the fractures. Comparing the effective continuum calculations with the results for the unfractured case (Fig. 9), it is seen that allowance for gas flow in the fractures causes a moderate increase in heat pipe length (Fig. 10), while additional allowance for liquid flow in the fractures gives dramatic effects (Fig. 11). In the latter case heat pipe conditions extend all the way to the heat source. With no dried conductive zone present, temperatures remain constrained near 100 °C. For case F the constant relative permeabilities allow direct integration of (7).

$$\omega\delta(r_i) = \frac{f(S_b) - f(0)}{\frac{1}{k_{rg}} + \frac{\beta}{k_{rl}}} \tag{15}$$

Comparison with Numerical Simulations

The numerical model TOUGH [19, 20] has been used to study the transient development of heat pipes, and to verify the analytical solutions presented above for the steady state. TOUGH (Transport Of Unsaturated Groundwater and Heat) calculates the two-phase flow of air and water in gaseous and liquid phases together with heat flow in a fully coupled way. The governing equations account for gaseous diffusion and Darcy flow with relative permeability and capillary pressure effects. Vaporization and condensation with latent heat effects along with conductive and convective heat flow are included in the energy balance. Water, air, and rock are assumed to be in local thermodynamic equilibrium at all times. The flow domain can include liquid, gaseous, and two-phase regions. Material properties vary with temperature and pressure in a realistic way. TOUGH employs an integral finite-difference method which is applicable for one-, two-, or three-dimensional flow problems in porous or fractured porous media. The

governing mass- and energy-balance equations are strongly nonlinear and are solved completely simultaneously, using Newton-Raphson iteration.

A one-dimensional radial calculational mesh with 50 elements is used to calculate $S(r)$, $P(r)$, $P_a(r)$, and $T(r)$ around a heat source for Case A (see Tables 1–3). The parameters in the left-hand column of Table 1 vary with temperature in TOUGH, but are considered constants for the analytical solution. Because the heat pipe is nearly isothermal, this difference is not significant [21]. Further, because the analytical solution does not consider air in the heat pipe region, we set the coefficient of binary diffusion to zero in the simulations. The innermost element of the mesh, $0<r<0.2$ m includes the heat source, with strength $Q = 500$ W/m. The mesh has a spacing of $dr = 0.1$ m where heat pipe effects are expected (0 to 4 m), and $dr = 0.6$ m for the outer conduction zone (4 to 10 m). Initial conditions are everywhere equal to P_b, T_b, and S_{lb}.

A calculation to steady state takes 300 time steps and requires 2.7 minutes of CPU time on a Cray X-MP. Fig. 12 shows the transient development of the heat pipe, with the analytical solution superimposed on the final frame, which shows steady state conditions. The agreement is quite good. In the numerical simulations liquid saturation shows a slight variation in the outer conduction region, indicating a weak heat pipe (liquid-vapor counterflow) process in the region with $T < T_{sat}(P_b)$. The analytical solution assumes constant saturation in the outer conduction region, leading to some difference between the analytical and simulated saturations at r_o. This difference is the source of the discrepancy between the analytical and simulated pressure profiles in the heat pipe region, and the slight difference in saturation profiles for $S>0.2$. If the analytical saturation at r_o is arbitrarily set to match the numerically simulated value there, then the analytical pressure profile matches the simulated one closely, and the analytical and simulated saturation profiles for $S>0.2$ agree well. By using a finer mesh, the numerically simulated saturation profile matches the analytical one closely for $S<0.2$, near r_i. Fig. 13 shows the analytical solution and the numerically simulated

results for a mesh with 132 elements, with finest resolution, dr =0.01 m, around r_i. This simulation would be quite expensive if it began with uniform initial conditions as the previous simulation did; instead it begins with the final conditions simulated by the 50 element mesh. This progression from coarse to fine calculational mesh provides an efficient way to utilize numerical models in conjunction with analytical solutions. Also shown in Fig. 13 are the results of a simulation including binary diffusion. Departures from the no-binary-diffusion simulation are small, and limited to the vicinity of r_o.

For the linear geometry case the treatment is similar, and an equally good match was found [20] between the numerically simulated results and the analytical solution.

Conclusions

Under steady state conditions three domains may exist around a cylindrical heat source emplaced in a partially saturated geological medium: a vapor-phase inner conduction zone, a two-phase heat pipe region, and a liquid water/air outer conduction zone. A heuristic model of mass and energy transport has been used to develop approximate analytical solutions for pressure, temperature, and liquid saturation profiles around the heat source. The accuracy of these solutions has been verified by means of numerical simulations. They offer a convenient means for addressing the important question of whether or not the vicinity of the heat source will dry up.

The extent of the heat pipe region can be much greater for radial geometry than for linear geometry, a consequence of the decrease in flow rate per unit area that occurs with radial distance. Because fluxes diminish with radial distance, smaller pressure gradients are needed to drive them. This leads to a smaller capillary pressure gradient, resulting in a smaller saturation gradient and a longer two-phase zone.

The characteristic curves for relative permeability and capillary pressure also have a strong impact on the extent of the heat pipe region. Fractured/porous media provide conditions which are favorable for heat pipe development, namely, large permeability in

the fractures and strong capillary effects in the porous matrix.

Future work plans include a study of the transient pressure, temperature, and saturation profiles that develop following emplacement of a heat source.

Acknowledgements

The careful review of this work by Y. W. Tsang and J. S. Y. Wang is gratefully appreciated. This work was supported, in part, by the Waste Management Branch, Division of Radiation Programs and Earth Sciences, Office of Nuclear Regulatory Research, U.S. Nuclear Regulatory Commission; and the U.S. Department of Energy under Contract No. DE-AC03-76SF00098.

Appendix A: Saturation Variation in the Heat Pipe Region

To determine $S(r)$ in the heat pipe region $r_i \leq r \leq r_o$, we begin with Darcy's law, modified for two-phase flow

$$\dot{m}_l = -\frac{kk_{rl}}{\nu_l}\frac{dP_l}{dr} \tag{A.1}$$

$$\dot{m}_v = -\frac{kk_{rv}}{\nu_v}\frac{dP_v}{dr} \tag{A.2}$$

where the subscripts v and l refer to vapor and liquid phases, respectively, $\dot{m}$ is mass flow rate per unit area, k is absolute permeability, k_r is the relative permeability of each phase, and ν is kinematic viscosity. Liquid pressure is less than vapor pressure because of the addition of the (negative) capillary pressure, P_{cap}

$$P_l = P_v + P_{cap} \tag{A.3}$$

so we may write

$$\frac{dP_{cap}}{dr} = \frac{dP_l}{dr} - \frac{dP_v}{dr} \tag{A.4}$$

Under steady state conditions, liquid and vapor flows are equal in magnitude and opposite in direction

$$\dot{m}_l + \dot{m}_v = 0 \tag{A.5}$$

For conditions of interest in nuclear waste isolation, heat fluxes are relatively small, so that temperature and pressure gradients in the heat pipe region are also small, and conductive heat flow there can be neglected. As a consequence, evaporation and condensation take place only at the hot and cold ends, respectively, of the heat pipe. The convective heat flux, q, is given by

$$q = \dot{m}_v h_{vl} \tag{A.6}$$

where h_{vl} is the latent enthalpy of vaporization of the liquid. For linear geometry, q is a constant, but for radial geometry q is a function of r, given by

$$q = \frac{Q}{2\pi r} \tag{A.7}$$

where Q is the constant heat source strength.

Substituting (A.1), (A.2), (A.5), (A.6), and (A.7) into (A.4) gives

$$\frac{dP_{cap}}{dr} = \frac{Q}{2\pi r k h_{vl}} \left(\frac{\nu_v}{k_{rv}} + \frac{\nu_l}{k_{rl}} \right) \tag{A.8}$$

Following Udell [8], we rewrite equation (A.8) in nondimensional form as

$$\frac{df}{d\delta} = -\omega \left(\frac{1}{k_{rv}} + \frac{\beta}{k_{rl}} \right) \tag{A.9}$$

where

$$f = \frac{P_{cap}}{P_{c0}} \tag{A.10}$$

$$\delta = \frac{r_o}{P_{c0}} (\rho_l - \rho_v) g \ln(r_o / r) \tag{A.11}$$

$$\omega = \frac{Q \nu_v}{2\pi r_o k h_{vl} (\rho_l - \rho_v) g} \tag{A.12}$$

$$\beta = \frac{\nu_l}{\nu_v} \tag{A.13}$$

Here P_{c0} is a (negative) reference pressure for a particular capillary pressure function, ρ is density, and g is gravitational acceleration. Equations (A.9) through (A.13) are identical to those for the linear heat pipe [8], except for the definitions of δ and ω (equations A.11 and A.12).

Equation (A.9) describes the variation of non-dimensional capillary pressure f with non-dimensional radial distance δ. Since we want an expression for the variation of saturation S with δ, we need to write (A.9) in terms of S. The relative permeabilities, k_{rv} and k_{rl}, and the non-dimensional capillary pressure, f, are all assumed to be functions of S only, so $df/d\delta$ may be written as

$$\frac{df}{d\delta} = \frac{df}{dS} \cdot \frac{dS}{d\delta} = f' \cdot \frac{dS}{d\delta} \tag{A.14}$$

where the notation $f' = df/dS$ is used. Hence (A.9) may be written as

$$\frac{dS}{d\delta} = \frac{\omega\left(\frac{1}{k_{rv}} + \frac{\beta}{k_{rl}}\right)}{-f'} \tag{A.15}$$

Equation (A.15) gives the fundamental relationship between scaled saturation S and non-dimensional length δ for the steady state of a heat pipe in one-dimensional radial geometry.

Table 1. Material properties (at $T = 101\,^\circ$C).

β	=	0.0142			
ν_v	=	18.9×10^{-6} m^2/sec	K_b	=	1.07 W/m °C
h_{vl}	=	2.257×10^{6} J/kg	K_v	=	0.582 W/m °C
σ	=	0.05878 N/m			

Table 2. Boundary conditions.

At r_b = 10 m	S_{lb} = 0.8
	P_b = 1 bar
	T_b = 26 °C
At r_c = 0.2 m	Q = 500 W/m

Table 3. Characteristic curves for relative permeability and capillary pressure dependence on saturation.

Case	Capillary Pressure	Relative Permeability
A†	$P_{cap} = P_{c0} f$ $P_{c0} = -\sigma(\phi/k)^{1/2}$ $f = a(1-S) + b(1-S)^2 + c(1-S)^3$ $a = 1.417,\ b = -2.12,\ c = 1.263$	$k_{rl} = S^3$ $k_{rg} = (1-S)^3$ $S_{lr} = 0.15,\ S_{ls} = 1.0$
B	Same as A	$k_{rl} = S$ $k_{rg} = 1-S$ $S_{lr} = 0.2,\ S_{ls} = 0.895$
C	Same as A	$k_{rl} = S^3$ $k_{rg} = a + bS + cS^2$ $a = 1.259,\ b = -1.7615,\ c = 0.5089$ $S_{lr} = 0.2,\ S_{ls} = 0.895$
D‡	$P_{cap} = P_{c0} f$ $P_{c0} = -13.93$ bars $f = (S^{-1/\lambda}-1)^{1-\lambda}$	$k_{rl} = \sqrt{S}\left[1-(1-S^{1/\lambda})^{\lambda}\right]^2$ $k_{rg} = 1 - k_{rl}$ $S_{lr} = 9.6\times10^{-4},\ S_{ls} = 1.0,\ \lambda = 0.45$
E	Same as D	$k_{rl} = \sqrt{S}\left[1-(1-S^{1/\lambda})^{\lambda}\right]^2$ $k_{rg} = 3067$ $S_{lr} = 9.6\times10^{-4},\ S_{ls} = 1.0,\ \lambda = 0.45$
F	Same as D	$k_{rl} = 90.65$ $k_{rg} = 2976$

† after Udell [8]
‡ after Hayden et al. [10]

References

1. D. E. White, L. J. P. Muffler and A. H. Truesdell. Vapor-dominated hydrothermal systems compared with hot-water systems. *Economic Geol.*, **66**(1), 75-97 (1971).

2. G. Schubert and J. M. Straus. Steam-water counterflow in porous media. *J. Geophys. Res.*, **84**(B4), 1621-1628 (1979).

3. K. Pruess. A quantitative model of vapor dominated geothermal reservoirs as heat pipes in fractured porous rock. *Transactions, Geoth. Res. Council*, **9**, part II, 353-361 (1985).

4. V. Dhir and I. Catton. Dryout heat fluxes for inductively heated particulate beds. *J. Heat Transfer*, **99**, 250-256 (1977).

5. H. C. Hardee and R. H. Nilson. Natural convection in porous media with heat generation. *Nuclear Sci. and Eng.*, **63**, 119-132 (1977).

6. Y. Ogniewicz and C. L. Tien. Porous heat pipe. In Heat transfer, thermal control, and heat pipes, W. B. Olstad, Ed., Vol. 70, Progress in astronautics and aeronautics, M. Summerfield, Series Ed., AIAA, New York. Presented as paper 79-1093, AIAA 14th Thermophysics Conf., Orlando, Florida, June (1979).

7. H. H. Bau and K. E. Torrance. Boiling in low-permeability porous materials. *Int. J. Heat Mass Transfer*, **25**(1), 45-55 (1982).

8. K. S. Udell. Heat transfer in porous media considering phase change and capillarity—the heat pipe effect. *Int. J. Heat Mass Transfer* **28**(2), 485-495 (1985).

9. K. Pruess, Y. W. Tsang and J. S. Y. Wang. Numerical studies of fluid and heat flow near high-level nuclear waste packages emplaced in partially saturated fractured tuff. *Rep. LBL-18552*, Lawrence Berkeley Laboratory, Berkeley, Calif. (1984).

10. N. K. Hayden, J. K. Johnstone and R. R. Peters. Parameters and material properties for hydrologic modeling of the Topopah Spring unit. Memo to distribution, Sandia National Laboratories, September 27 (1983).

11. W. H. Somerton, J. A. Keese and S. L. Chu. Thermal behavior of unconsolidated oil sands. *Pap. SPE-4506*, presented at 48th Annual Fall Meeting of the Society of Petroleum Engineers, Las Vegas (1973).

12. W. H. Somerton, A. H. El-Shaarani and S. M. Mobarak. High temperature behavior of rocks associated with geothermal type reservoirs. *Pap. SPE-4897*, presented at 44th Annual California Regional Meeting of the Society of Petroleum Engineers, San Francisco (1974).

13. *IMSL Library Edition 9 Reference Manual*, Ch. D, IMSL, Houston (1982).

14. I. Fatt and W. A. Klikoff. Effect of fractional wettability on multiphase flow through porous media. AIME Technical Note #2043, *AIME Trans.* **216**, 246 (1959).

15. M. C. Leverett. Capillary behavior in porous solids. *AIME Trans.* **142**, 152-169 (1941).

16. M. R. J. Wyllie. Relative permeability. In *Petroleum Production Handbook*, Frick ed., Vol. 2, Ch. 25, McGraw-Hill, New York (1962).

17. A. K. Verma, K. Pruess, C. F. Tsang and P. A. Witherspoon. A study of two-phase concurrent flow of steam and water in an unconsolidated porous medium. Presented at the 23rd ASME/AIChE National Heat Transfer Conference, Denver, August (1985).

18. M. Th. van Genuchten. A closed-form equation for predicting the hydraulic conductivity of the unsaturated soils. *Soil Sci. Soc. Am. J.*, **44**, 892-898 (1980).

19. K. Pruess. TOUGH—A numerical model for strongly heat driven flow in partially saturated media. In Earth Sciences Division Annual Report 1983, 39-41, *Rep. LBL-16920*, Lawrence Berkeley Laboratory, Berkeley, Calif. (1984).

20. K. Pruess. TOUGH user's guide. *Rep. LBL-20700*, Lawrence Berkeley Laboratory, Berkeley, Calif. (1986).

21. C. Doughty and K. Pruess. Numerical modeling of a porous heat pipe: comparison with a semianalytical solution. In Earth Sciences Division Annual Report 1986, *Rep. LBL-22090*, Lawrence Berkeley Laboratory, Berkeley, Calif. (1987).

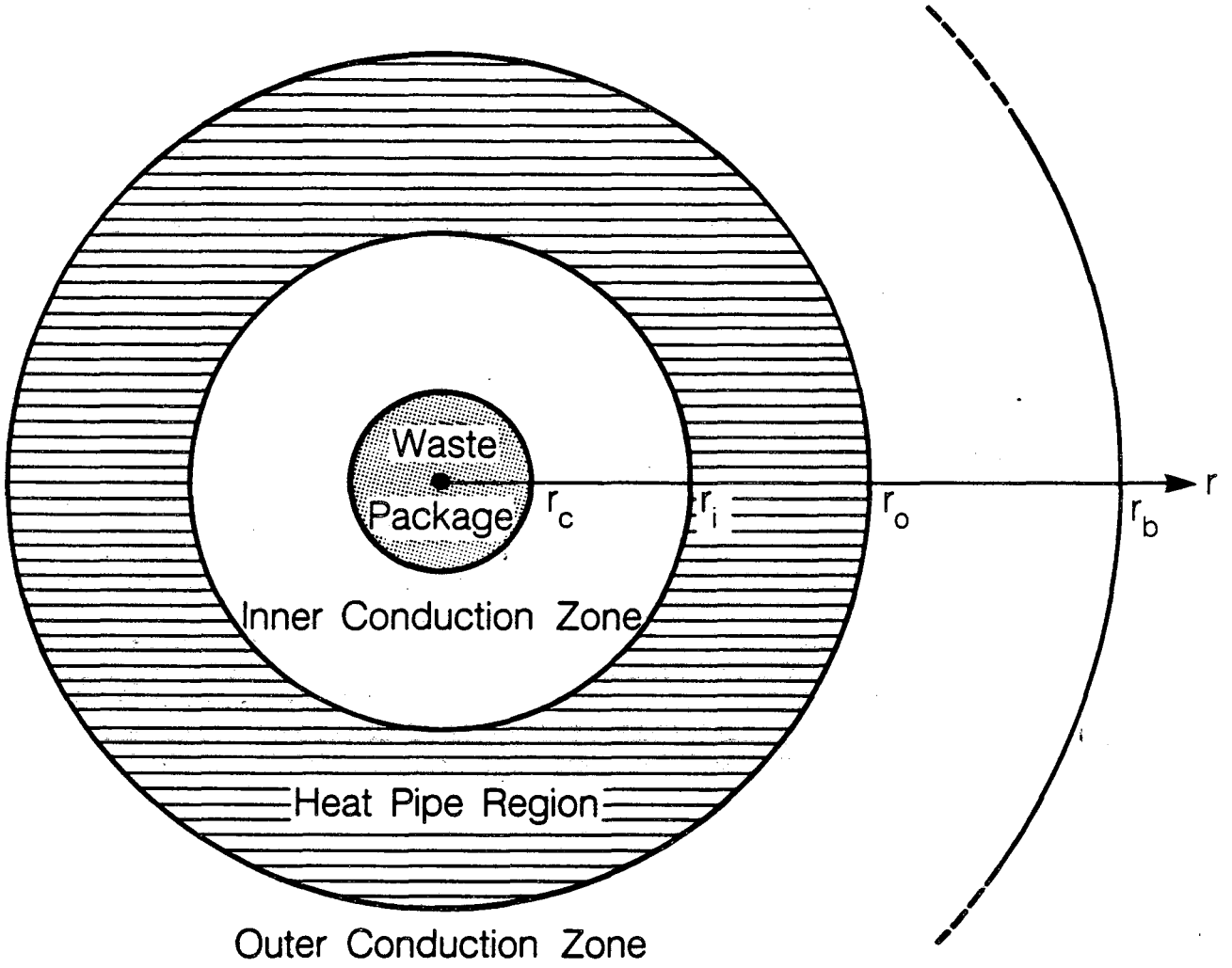

XBL 8611-12738

Fig. 1. Schematic of heat transfer regimes in plane perpendicular to the axis of the waste packages (not to scale).

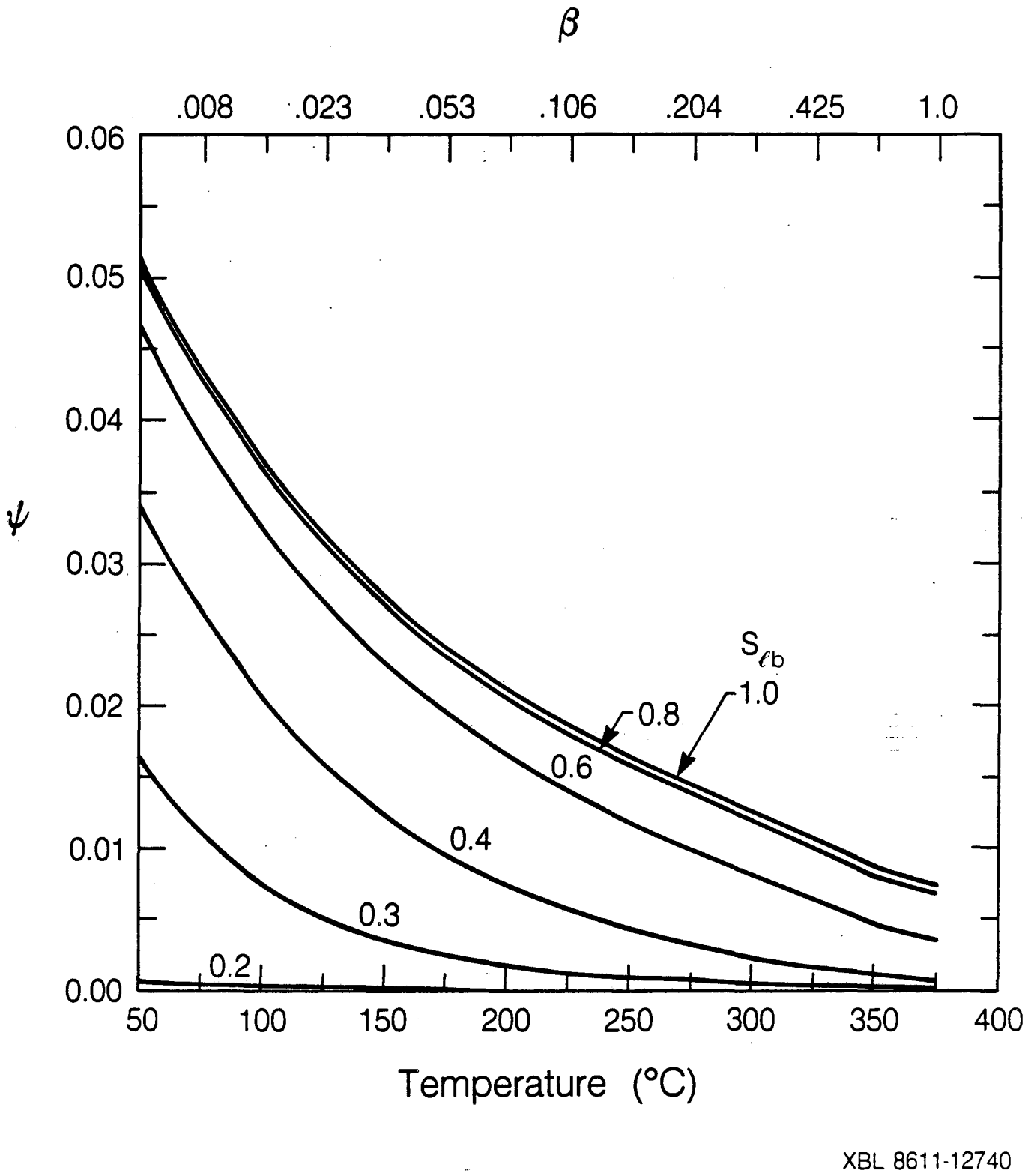

XBL 8611-12740

Fig. 2. The function $\psi(\beta, S_b)$ for a range of temperatures and saturation boundary conditions, calculated using characteristic curves given in Table 1, case A.

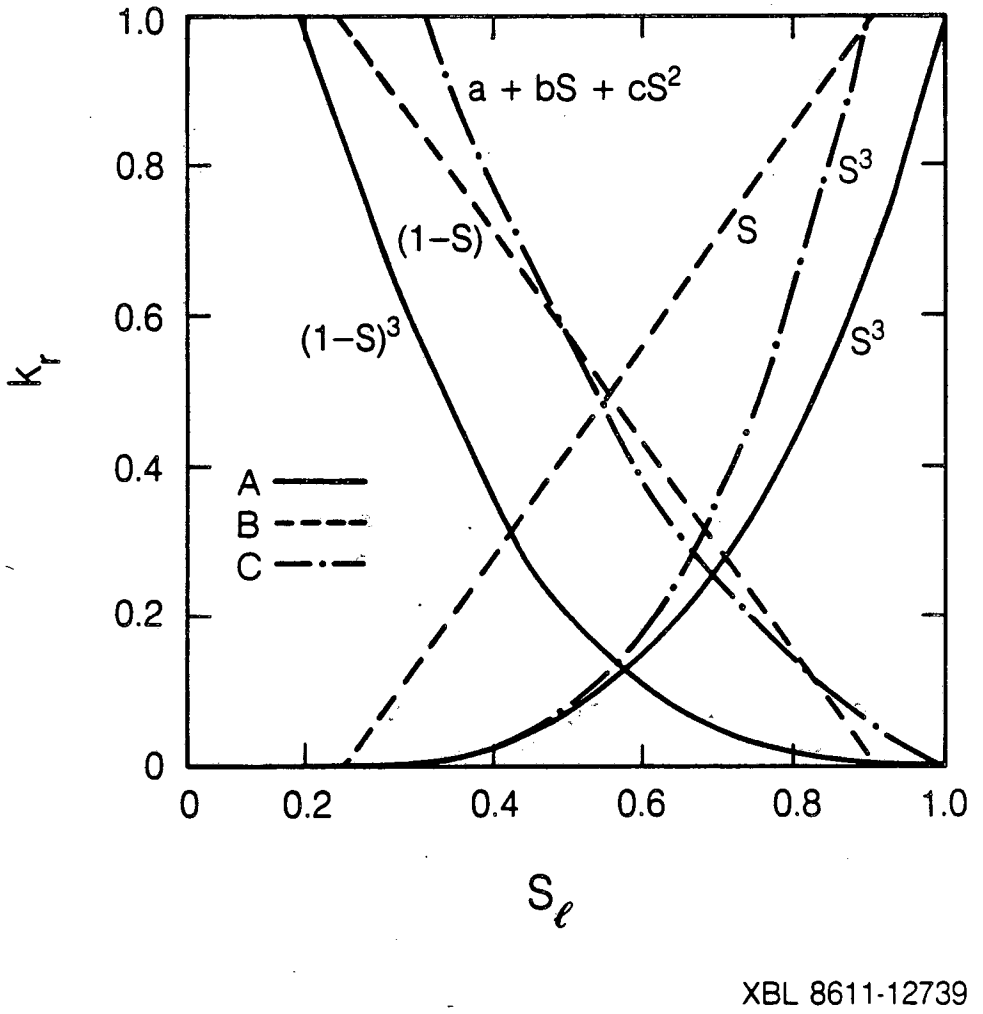

XBL 8611-12739

Fig. 3. Relative permeability curves for cases A–C.

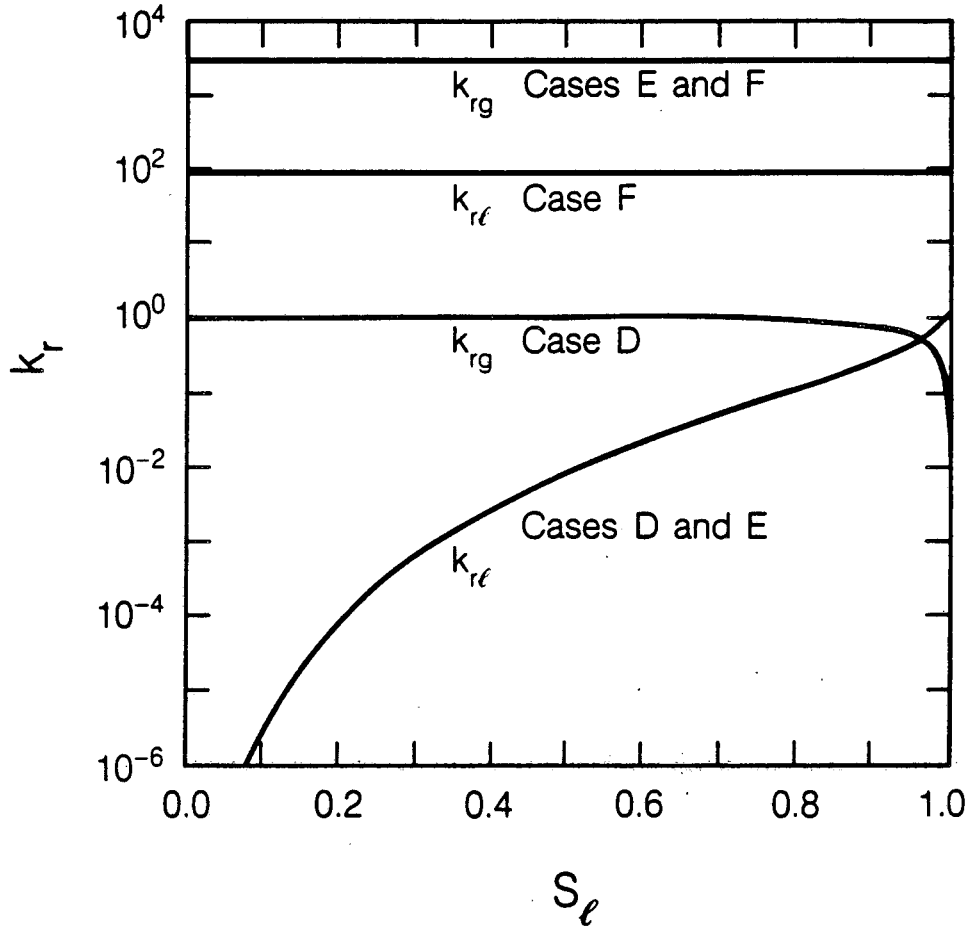

XBL 8611-12750

Fig. 4. Relative permeability curves for cases D–F.

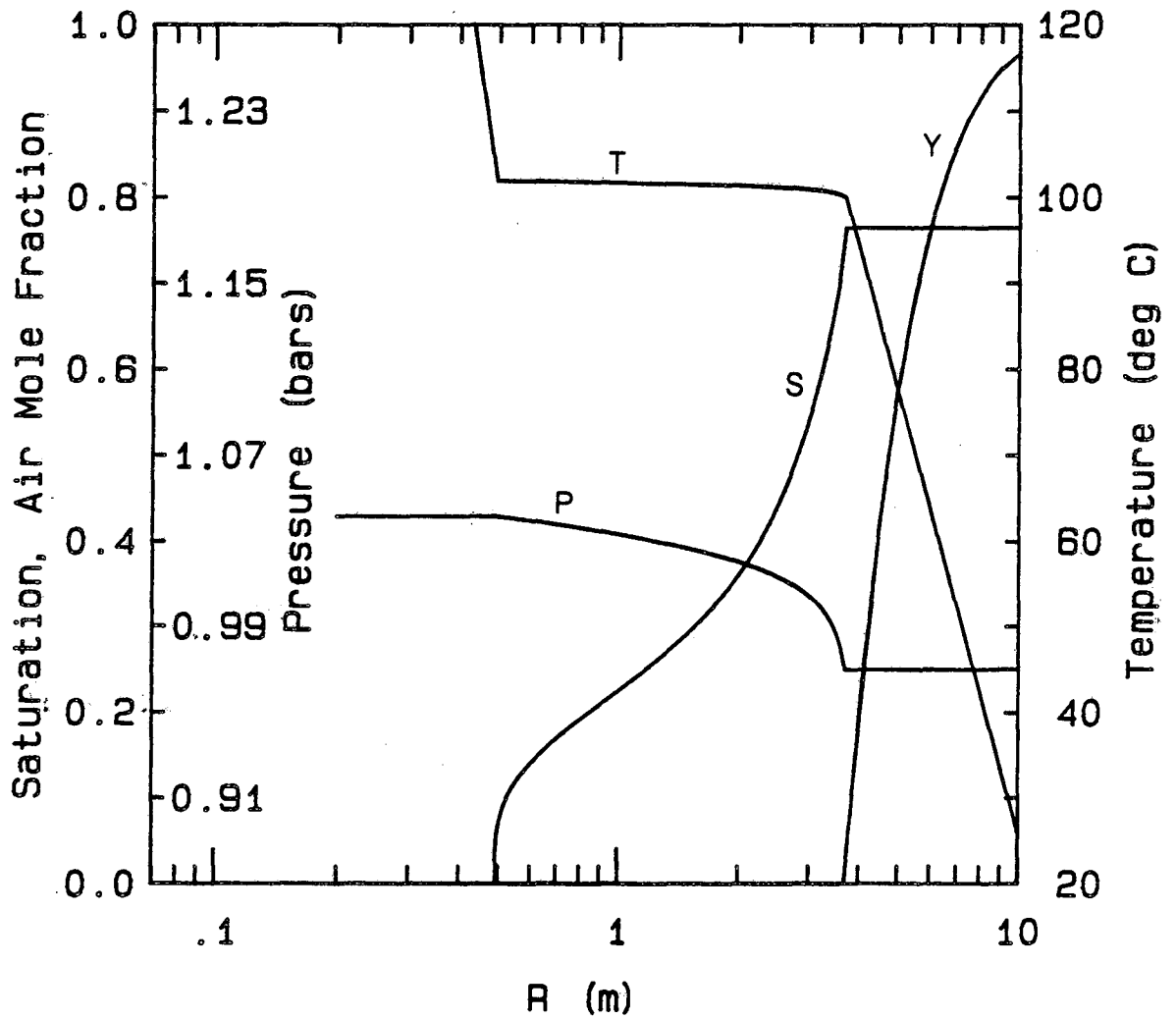

XBL 8611-12741

Fig. 5. Analytical solution for scaled saturation, pressure, temperature, and air mole fraction profiles, using characteristic curves from Table 1, case A, and S_{lb} =0.80.

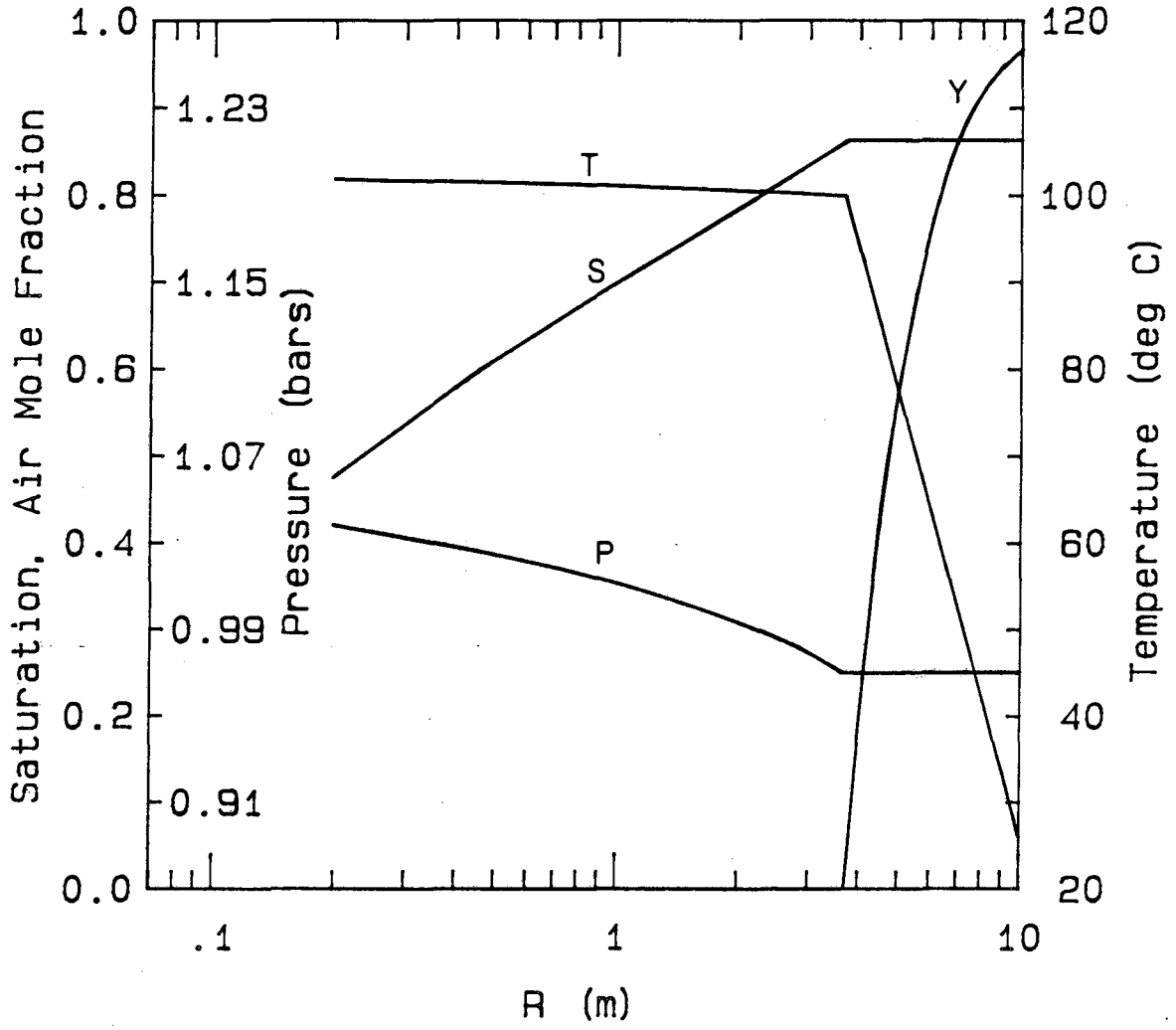

XBL 8611-12742

Fig. 6. Scaled saturation, pressure, temperature, and air mole fraction profiles for case B and S_{lb} =0.80.

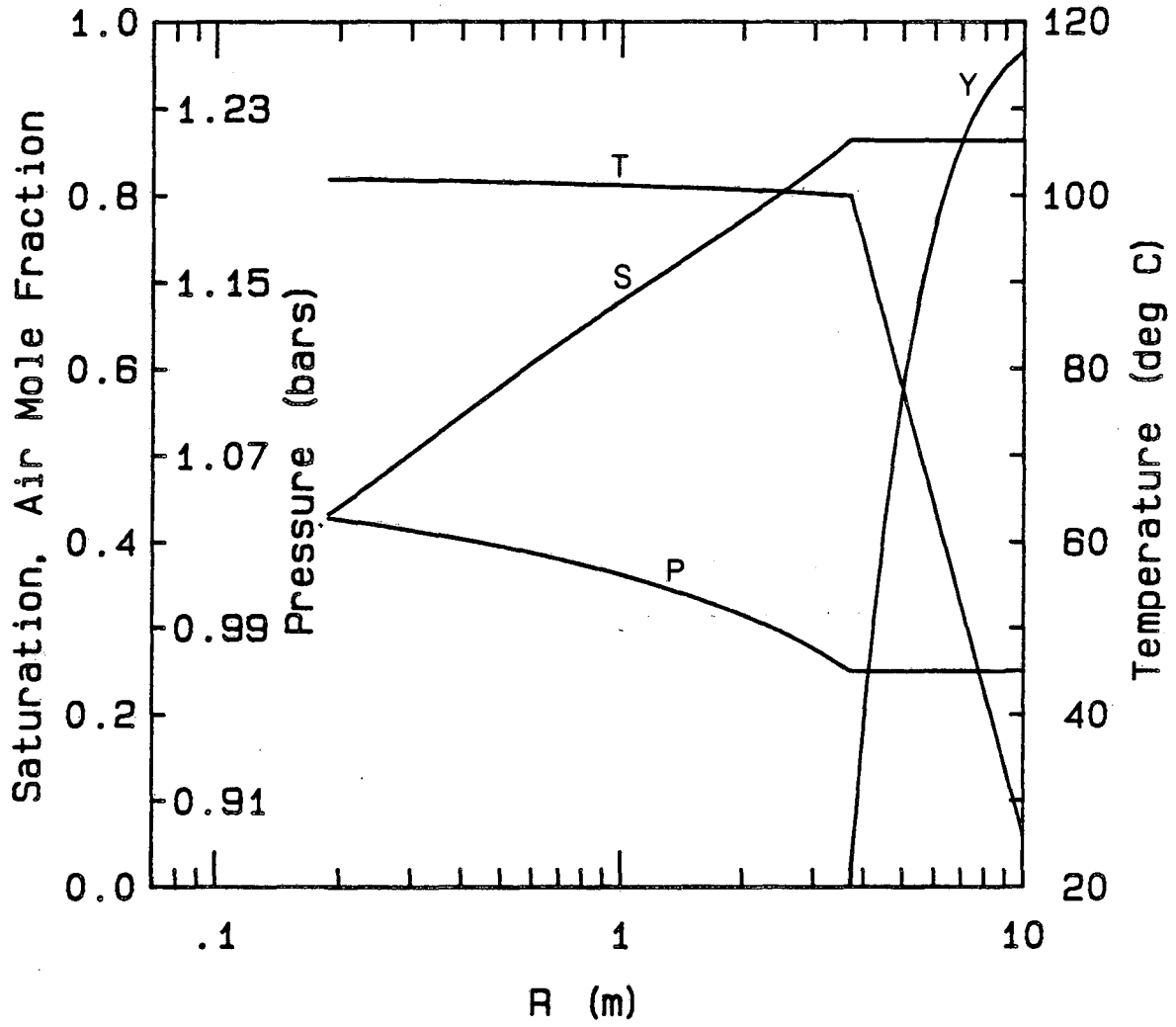

XBL 8611-12743

Fig. 7. Scaled saturation, pressure, temperature, and air mole fraction profiles for case C and S_{lb} =0.80.

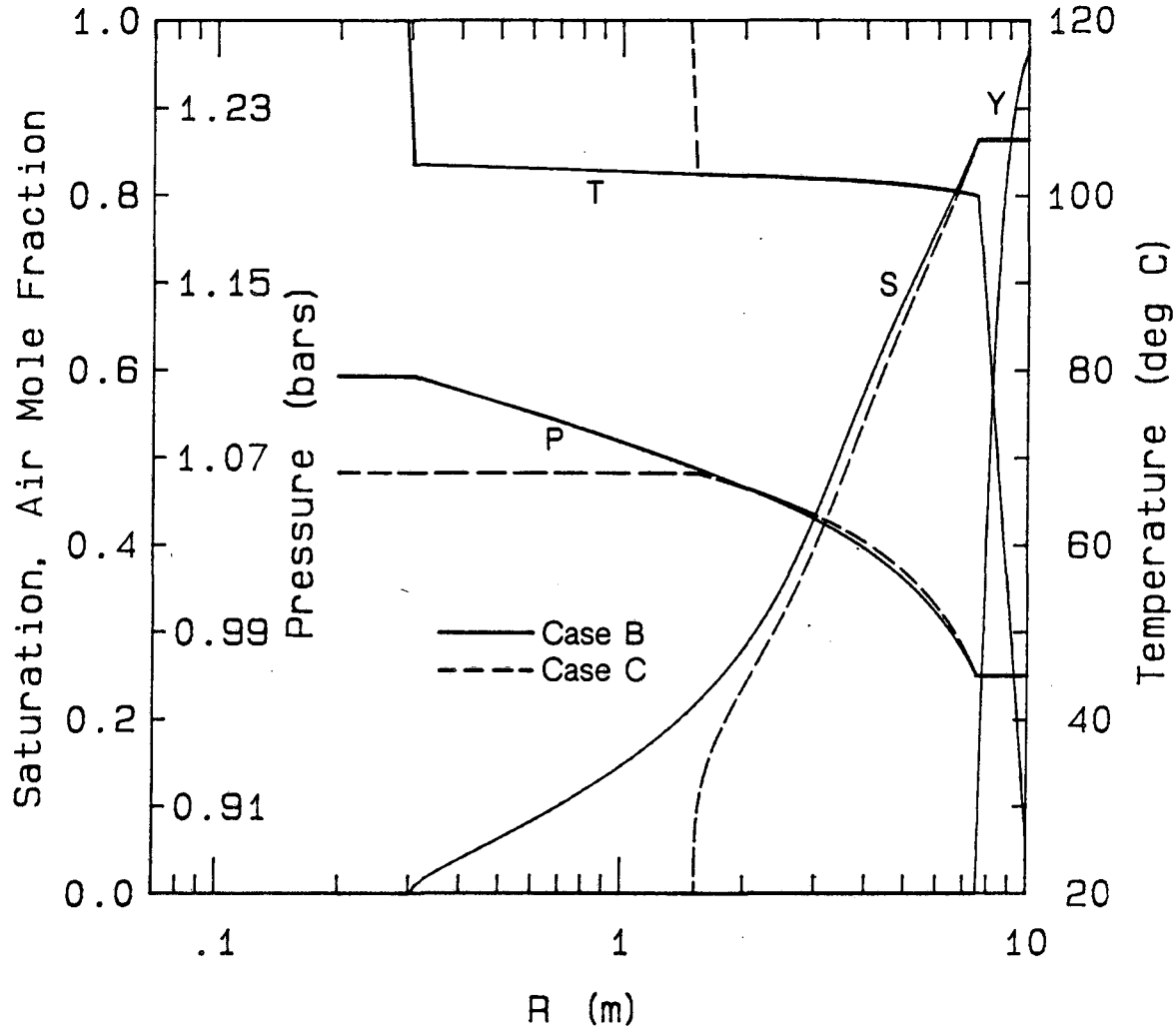

XBL 8611-12744

Fig. 8. Scaled saturation, pressure, temperature, and air mole fraction profiles for cases B and C with S_{lb} =0.80 and Q = 1750 W/m.

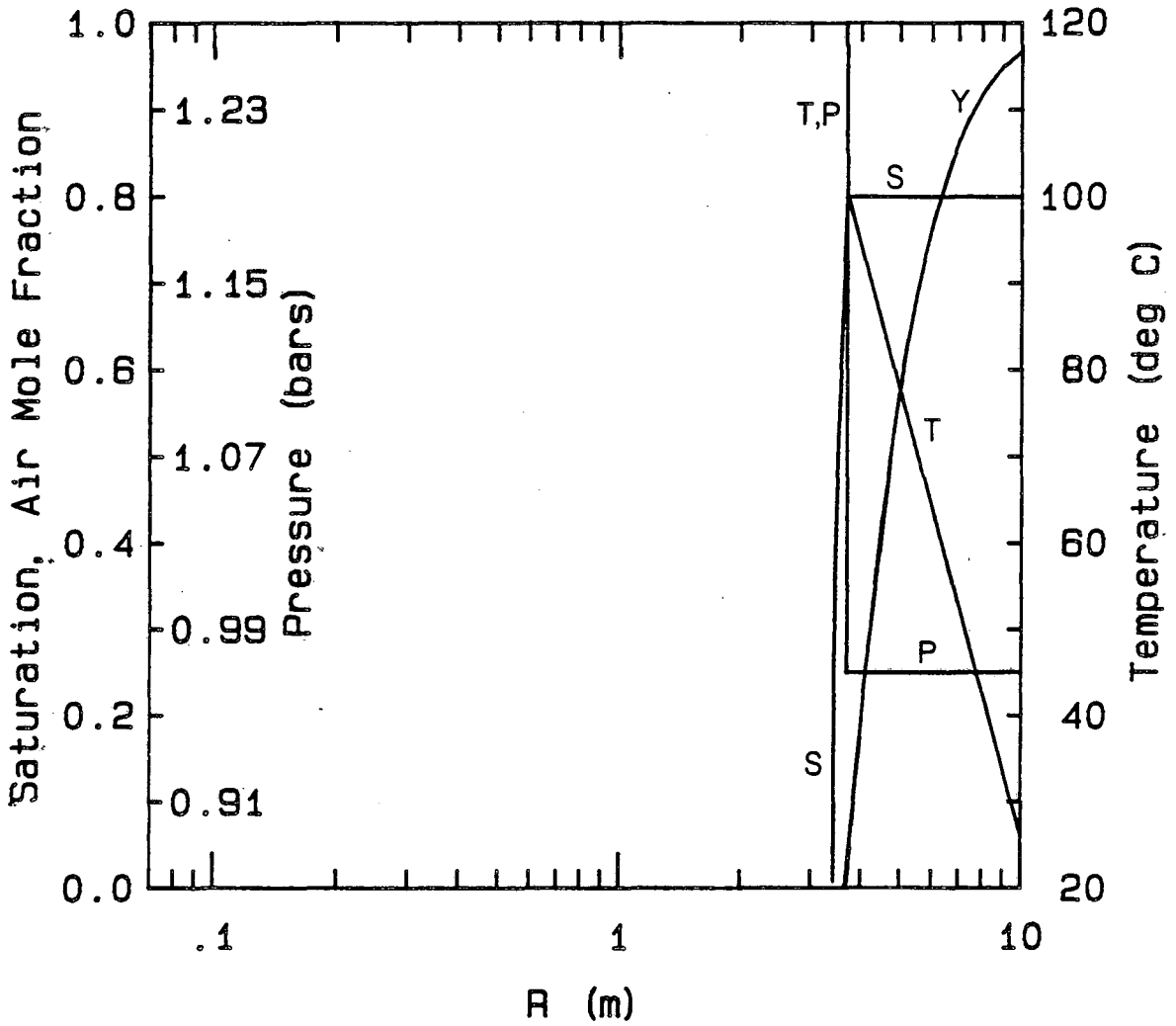

XBL 8611-12745

Fig. 9. Scaled saturation, pressure, temperature, and air mole fraction profiles for case D and S_{lb} =0.80.

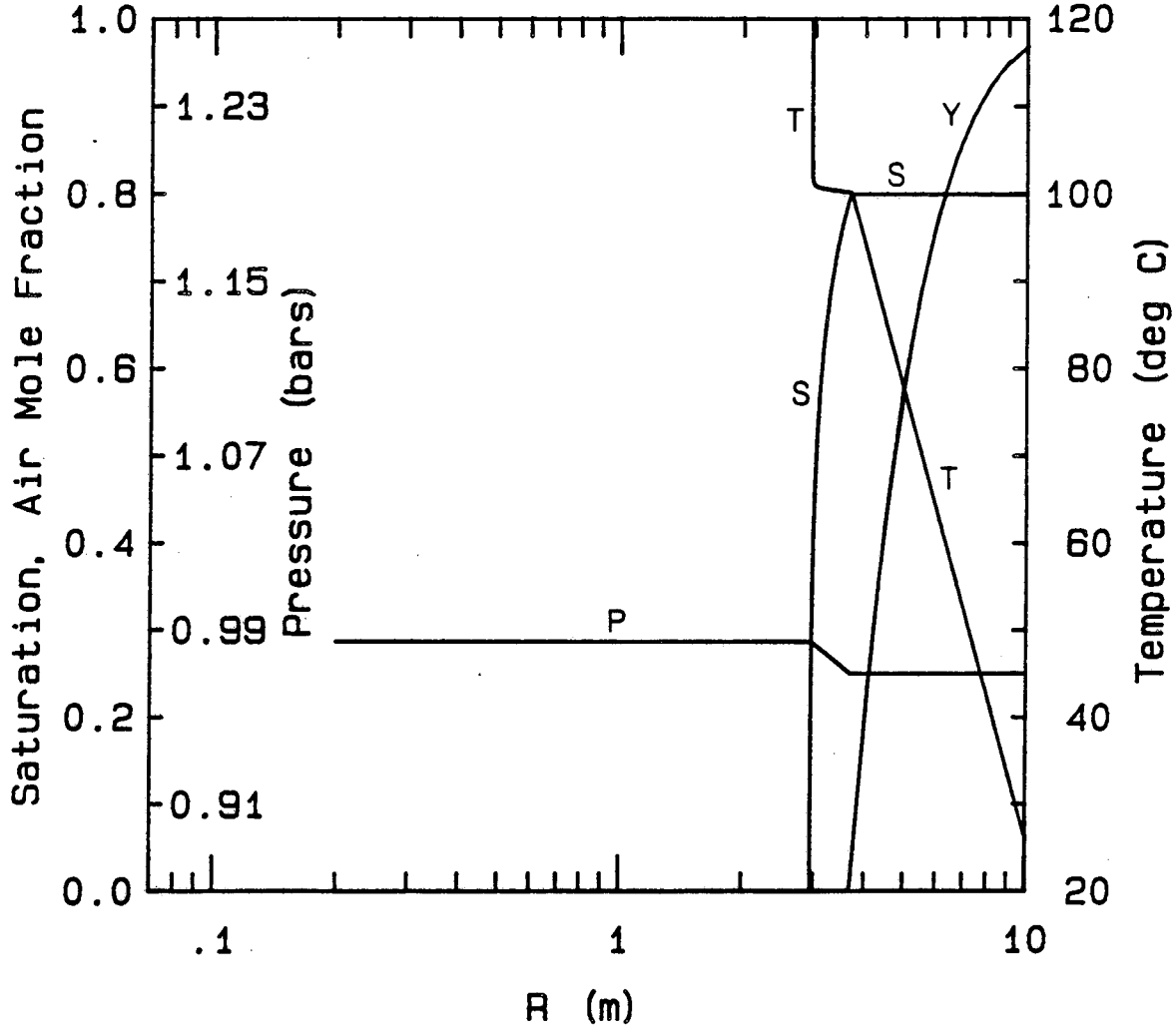

XBL 8611-12746

Fig. 10. Scaled saturation, pressure, temperature, and air mole fraction profiles for case E and S_{lb} =0.80.

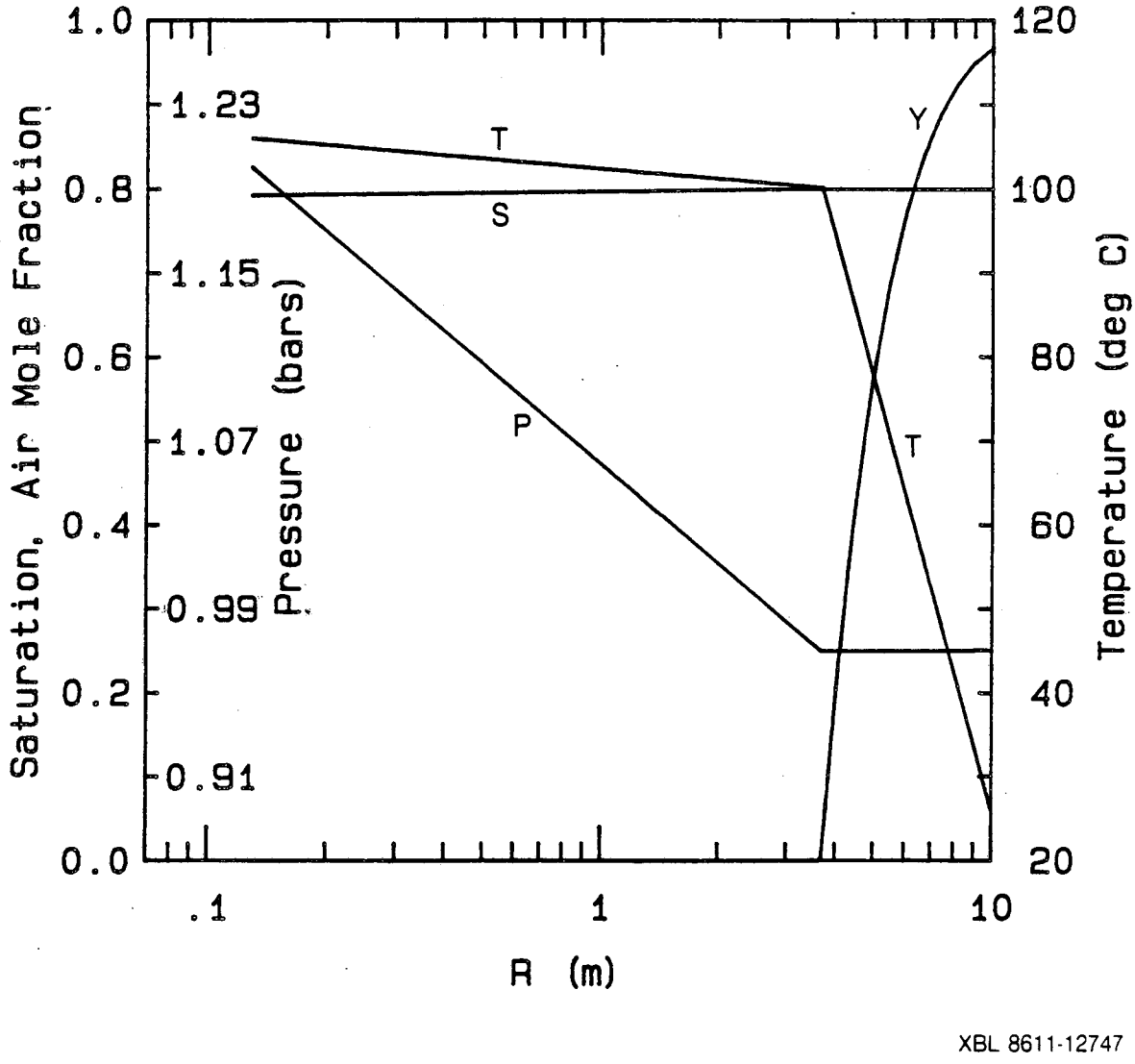

XBL 8611-12747

Fig. 11. Scaled saturation, pressure, temperature, and air mole fraction profiles for case F and S_{lb} =0.80.

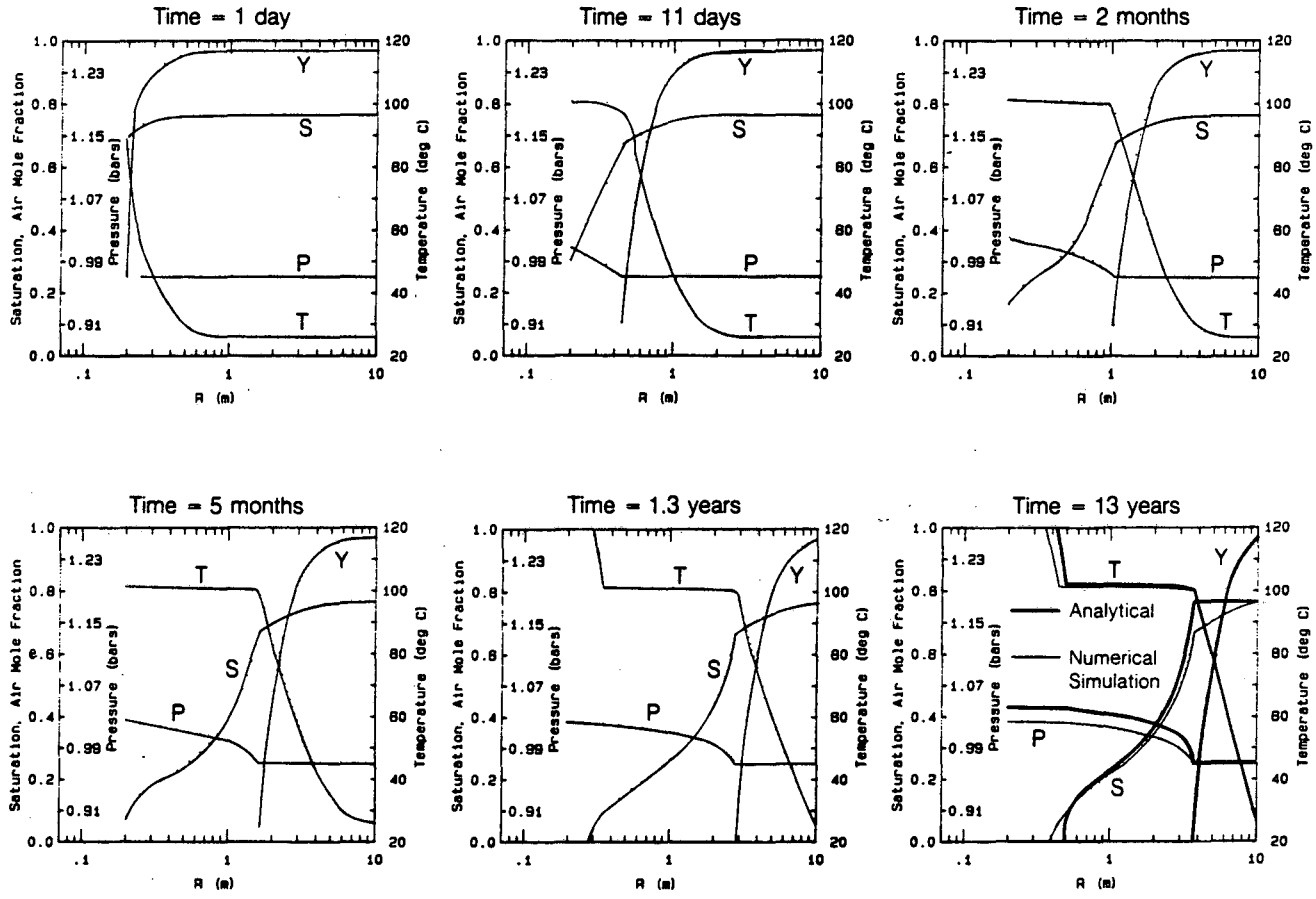

Fig. 12. Numerically simulated scaled saturation, pressure, temperature, and air mole fraction profiles at various times. For steady-state conditions, numerical and analytical solutions are both shown.

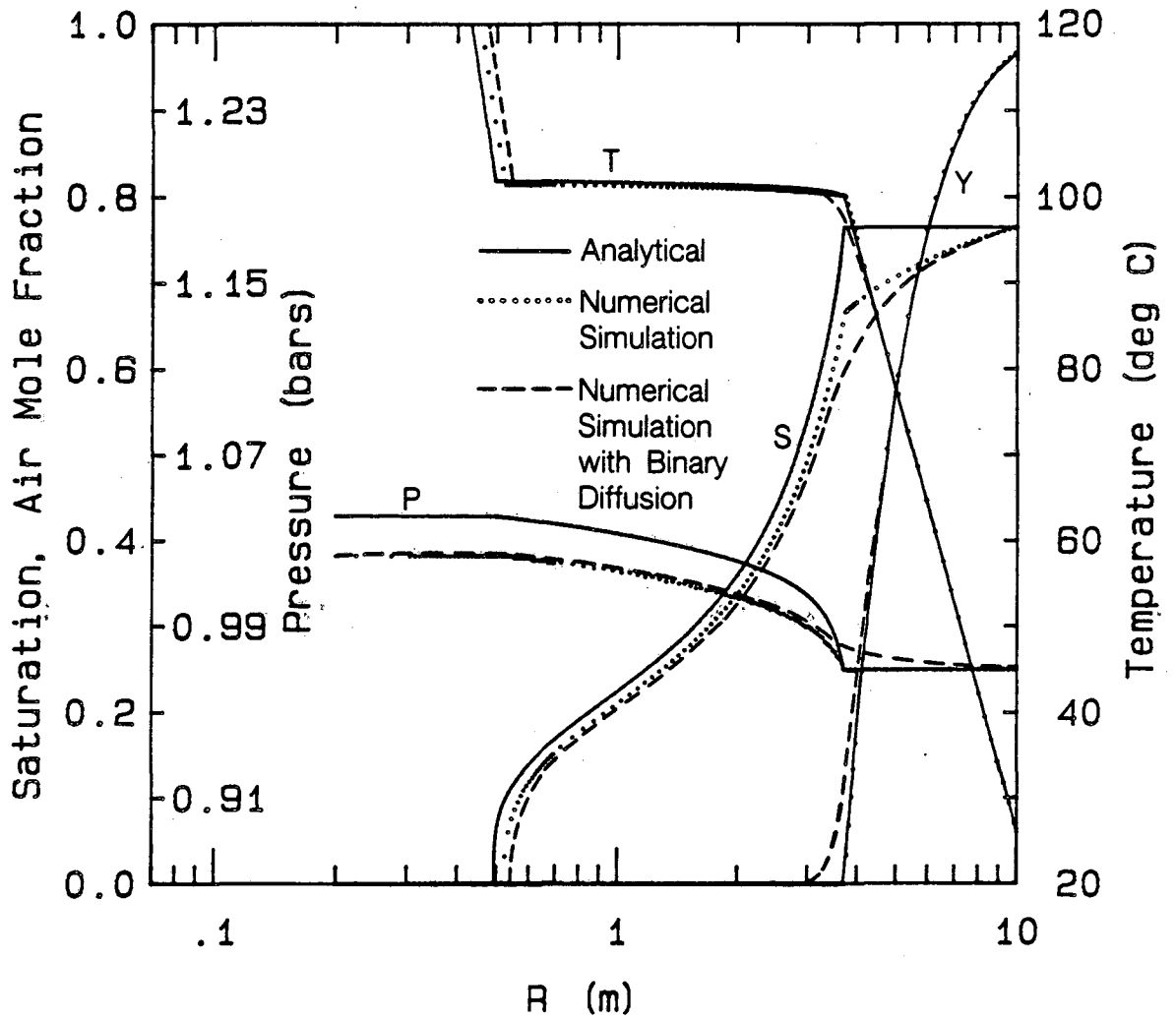

XBL 8611-12748

Fig. 13. Steady state profiles simulated numerically using a fine mesh, compared with the analytical solution. Profiles for a simulation including binary diffusion are also shown.

This report was done with support from the Department of Energy. Any conclusions or opinions expressed in this report represent solely those of the author(s) and not necessarily those of The Regents of the University of California, the Lawrence Berkeley Laboratory or the Department of Energy.

Reference to a company or product name does not imply approval or recommendation of the product by the University of California or the U.S. Department of Energy to the exclusion of others that may be suitable.

LAWRENCE BERKELEY LABORATORY
TECHNICAL INFORMATION DEPARTMENT
UNIVERSITY OF CALIFORNIA
BERKELEY, CALIFORNIA 94720